Article

Not peer-reviewed version

Developing Preventative Strategies to Mitigate Thermal Runaway in NMC532-Graphite Cylindrical Cells Using Forensic Simulations

Justin Holloway , Muinuddin Maharun , Irma Houmadi , Guillaume Remy , Louis Piper , Mark Williams , Melanie Jayne Loveridge *

Posted Date: 2 February 2024

doi: 10.20944/preprints202402.0095.v1

Keywords: catastrophic failure; lithium-ion battery; thermal runaway; cylindrical cell design; battery safety

Article

Developing Preventative Strategies to Mitigate Thermal Runaway in NMC532-Graphite Cylindrical Cells Using Forensic Simulations

Justin Holloway [1], Muinuddin Maharun [1], Irma Houmadi [1], Guillaume Remy [1], Louis Piper [1,2], Mark A Williams [1] and Melanie Loveridge [1,2]

[1] WMG, The University of Warwick, Coventry, CV4 7AL, UK
[2] The Faraday Institution, Quad One, Becquerel Avenue, Harwell Campus, Didcot OX11 0RA, UK
* Correspondence: Mel Loveridge, Address: WMG, The University of Warwick, Coventry, CV4 7AL, United Kingdom; Telephone: +44 (0) 24 7615 1043; Fax: +44 (0)24 7646 1606; Email address: m.loveridge@warwick.ac.uk

Abstract: The ubiquitous deployment of Li-ion batteries (LIBs) in more demanding applications has reinforced the need to understand root-causes of thermal runaway. Herein we perform a forensic simulation of a real-case failure scenario, using localised heating of $Li(Ni_{0.5}Mn_{0.3}Co_{0.2})O_2$ versus graphite 18650 cylindrical cells. This study determined the localised temperatures that would lead to venting and thermal runaway of these cells, as well as correlating the gases produced as a function of degradation pathway. Catastrophic failure, involving melting (with internal cell temperatures exceeding 1085°C), deformation and ejection of cell componentry, was induced by locally applying 200 °C and 250 °C to a fully charged cell. Conversely, catastrophic failure was not observed when the same temperatures were applied to the cells at lower state of charge (SOC). This work highlights the importance of SOC, chemistry and heat in driving the thermal failure mode of Ni-rich LIB cells, allowing for a better understanding of battery safety and associated design improvements.

Keywords: catastrophic failure; lithium-ion battery; thermal runaway; cylindrical cell design; battery safety

1. Introduction

Li-ion batteries have become the most convenient source of power for portable electronic applications since their launch in 1991[1]. Such uses, along with other consumer electronics now commonly use lithium-ion batteries (LIBs) but have increasingly received much attention in recent years regarding their safety parameters. They contain a flammable and toxic organic solvent electrolyte that can become gaseous with increases in temperature, and lead to cell venting [2,3]. In a worst-case scenario, they can also undergo catastrophic failure through thermal runaway (TR). The prevention of TR has become more vital than ever, as the technology is now pushed to the limits of power and energy density for some chemistries [4]. With LIBs increasingly employing larger cells and format dimensions to achieve higher energy densities. Examples of these include the BYD Blade cell which > 90 cm in length with a capacity of 202 Ah. As such, the mitigation of TR (or circumnavigating it entirely) has become paramount to ensure better safety. As temperatures increase, the carbonate electrolyte decomposes and can generate pressure increase within the battery, the extent of which determines whether a cell vents or enters into a thermal runaway (TR) condition [3]. TR is specifically brought about by a cascade of exothermic chain reactions, which dramatically increase the battery temperature, leading to uncontrollable temperature increases and eventual combustion [5]. Devising a means of reducing or eliminating key exothermic reactions during the early stages of TR is paramount to engineering improved safety into LIBs. Early detection systems have been developed that can now detect unique precursors to TR [6]. Any early detection mode will need to take into account the sequential stages of TR:

 doi:10.20944/preprints202402.0095.v1

The abuse condition → Gassing → Smoke generation → Fire

From the perspective of fire protection technology, development is needed to monitor real-time early-stage warnings. Whilst one of the functions of the battery management system (BMS) is to monitor state-of-health, it cannot monitor and alarm the early stages of TR [7]. Traditional BMS measurements of changes in battery voltage, current, temperature and other parameters could offer more predictive early-stage TR capability, if analysed more deeply, precisely and with improved hard or soft sensing accompaniments [8]. However, even the "best" BMSs that monitor voltage and external surface temperature of each cell are not capable of preventing TR propagation because they cannot track the fast-emerging adverse events in-real-time [9] which occur over a few seconds [10]. Detecting changes in cell volume and pressure have been used to avoid TR, e.g., most LIBs contain a safety vent, which is designed to release gases and avoid runaway. In cylindrical cells this vent is in the form of a concave domed disc at the top of the cell, that in the event of a pressure increase releases gases into the surroundings. There are a range of safety tests for batteries [11], designed to simulate situations during operation and are used as a method to validate safety. More specifically, there are environmental tests, such as climate chamber tests [12] which involves exposing the cell to temperatures up to 150°C for 10 minutes; passing the test requires the cell to not vent or undergo catastrophic failure. Given the many applications for batteries, such tests may not be able to cover every operational scenario, such as exposure to localised heating. With the drive for smaller but greater powered devices, this could result in poor design of ancillary electric circuitry whereby temperatures could exceed 150°C and for longer than 10 minutes. The benefit of forensic simulation approaches on real format batteries allows us to:

1. understand complex reaction pathways (with the aid of appropriate additional characterisation), and
2. provide learning into how to suppress TR following the onset of rapid deterioration of electrodes and electrolyte.

Deeper understandings from (i) can better inform the design and generation of improved materials and chemicals – ones that will better withstand conditions whereby accelerated degradation would ordinarily occur.

In addition to temperature, the SOC of a cell also has an impact on the likelihood of thermal runaway, relating to peak heat flux with higher SOC [13]. It is actually both the thermal stability of the cathode and SOC of the anode that are actually instrumental to the severity of thermal runaway in LIBs [14], with the anode and cathode active materials responsible for generating more heat at higher SOC [15]. Understanding the effects of SOC on the aging behaviour in LIBs can serve to extend the service life and also to increase their safer operation. As cells based on NMC532 versus graphite age, a consequence of this is Li inventory depletion, such that the operating voltage of the cathode steadily increases – a phenomenon referred to as electrode slippage [13]. This makes it easier to over-delithiate the cathode at higher SOC [16]. If too much Li is extracted from the NMC, the crystal structure becomes destabilised and starts to reduce at the particle surface – with resulting oxygen loss and exothermic reactions with the electrolyte [17,18]. On the other electrode side of the cell the lower cut-off potential is dominated by the anode voltage rise upon delithiation, facilitating an over-discharged condition at lower SOC [16]. An impact of this is a destabilised solid electrolyte interphase (SEI) [19] and the increased likelihood of gassing and capacity fade.

As the development of higher energy density cathode materials (with greater % of Ni) continues, so does the challenges of achieving greater thermal stability with these materials, a crucial performance and safety parameter. Since Ni can cycle between $Ni^{2+/3+}$ and $Ni^{3+/4+}$ redox couples without large variations in voltage, the evolution of higher Ni NMCs such as NMC532, 622 - and more recently 811 – became possible [20]. This followed the commercial success of the initial development and uptake of NMC 111 and 333. However, cells based on higher Ni layered oxides still suffer from fast capacity decay and low thermal-abuse tolerance at higher voltages [21]. The amount of side-reaction products has been observed to increase constantly, corresponding to more Ni content

 doi:10.20944/preprints202402.0095.v1

[22]. The average TR trigger temperature of NMC532 has been reported to be 244.1°C [23], and informed the conditions of this study.

Our methodology was chosen to mimic the conditions of a real event, whereby cylindrical cells were exposed to continual localised heat and charging which ultimately induced catastrophic failure (this event is summarised in Figure 1). The TR triggering event - dT/dt – for NMC532 is reported as 540.5°C min^{-1} (average of 3 cells) [23]. In the situation where the BMS is to prevent TR by activating a rapid cooling mechanism, an early-stage detection method is required to detect exotherms or alternatively to detect gas release in real time.

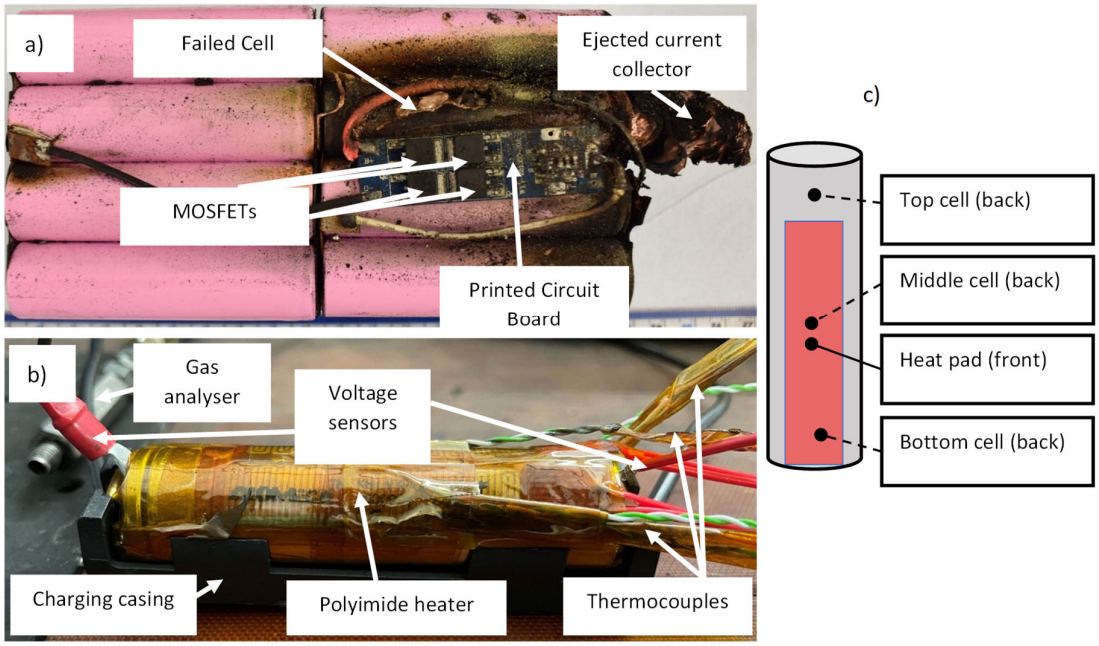

Figure 1. Images of: a) A real field failure situation b) Experimental setup to emulate the failure situation and c) location of TCs on an individual cell.

Here we demonstrate by forensic reconstruction how low SOC facilitates venting only (with applied temperatures up to 250°C), while high SOC facilitates venting and thermal runaway (at a lower applied temperature, 200°C). TR results in internal temperatures greater than 1000°C. We go further by demonstrating that at high SOC it is possible to avoid TR onset at venting by rapidly removing the heat source.

2. Experimental

Sets of three commercial LG 18650 cylindrical cells (nominal capacity 2.2 Ah and based on graphite – NMC-532 chemistry) were tested under two conditions. These involved a cell heating and charging test (henceforth referred to as low SOC test) and a charged cell heating test (henceforth referred to as high SOC test) respectively. The low SOC test involved charging cells from 0% SOC to 100% SOC using C/3 CC then CV to C/30 Whilst charging was undertaken cells had constant temperatures of 100°C, 150°C, 200°C or 250°C applied in localised areas for 3 hours. The high SOC test involved maintaining cells at 100% SOC and applying constant temperatures of 100°C, 150°C, 200°C and 250°C in a localised area for 3 hours. In both conditions the tests were stopped if the cell underwent catastrophic failure.

All testing was carried out in an abuse test chamber set at 25°C, with temperatures monitored using K-type thermocouples (TCs) connected to a Pico (TC-08) data logger. Cell voltage was monitored using a voltage sensor (TC-08 single channel terminal board). Cell charging and characterisation was carried out using a Maccor 4200 battery cycler. Localised heating was provided

 doi:10.20944/preprints202402.0095.v1

by an Omega polyimide flexible film heater (12.7 mm wide x 50.8 mm long and rated at 10 W). The heating temperature was further controlled using a proportional integral derivative (PID) controller based on an Arduino board. The controller regulated the supplied current to the heater based on temperatures logged via TC on the surface of the heater. Figure 1 shows a module failure situation from an internal case study using similar cells and experimental setup to emulate the failure situation.

Gases generated during testing were monitored using a Hiden gas analyser based on quadrupole mass spectroscopy (QMS). The measurement was taken in real-time, with the equipment nozzle placed approximately 15mm from the positive end of the cell, where the cell is known to house safety devices such as the current interrupt device (CID) and positive temperature coefficient (PTC) device.

CT scans were carried out using a ZEISS METROTOM scanner set to a resolution of 31µm; CT reconstruction software used was Metrotom OS. X-Ray Micro CT is non-destructive testing (NDT) using X-ray radiographs through 360° rotation creating a 3D volume allowing the visualisation of the internal structure of the cell [24]. The radiographs are then reconstructed using Metrotom OS to generate the rendered volume.

Cross sections of the cells were prepared using standard metallurgical techniques and etched using 1% Nital solution for 5 seconds. Optical micrographs were taken using a Nikon Eclipse LV150N microscope. Mechanical properties were obtained by hardness testing, performed using a Wilson VH3300 Automatic Hardness Tester. Vickers micro-hardness tests were carried out with a load of 0.1 kg and a dwell time of 15 s.

3. Results and Discussion

3.1. Temperature-Induced Venting Without Thermal Runaway: Low SOC Regime

A summary of thermal events observed from low SOC testing is shown by Table 1. Venting can be identified by the temperatures logged during testing and has been identified by way of the Joule Thomson cooling effect [25]. This is due to a change in temperature that accompanies the expansion of a gas without the production of work or transfer of heat.

Table 1. Summary of testing results.

Test	Temperature (°C)	Events
Low SOC	100	Nil
	150	Nil
	200	Venting only
	250	Venting only

The low SOC test did not induce thermal runaway and only resulted in venting. Figure 2 shows the typical temperatures measured during testing. As can be seen all cells were heated until the cell reached an equilibrium temperature whereby the rate of heat dissipation exceeded the rate of heat generation applied to the cell. The 200°C and 250°C samples vented at an SOC of 6% and 7% respectively. Cells at high SOC are tied to higher fire hazards; having more intense reactions and (flammable) gas generation [26]. Furthermore, increasing SOC increases the volume of gases released [27].

 doi:10.20944/preprints202402.0095.v1

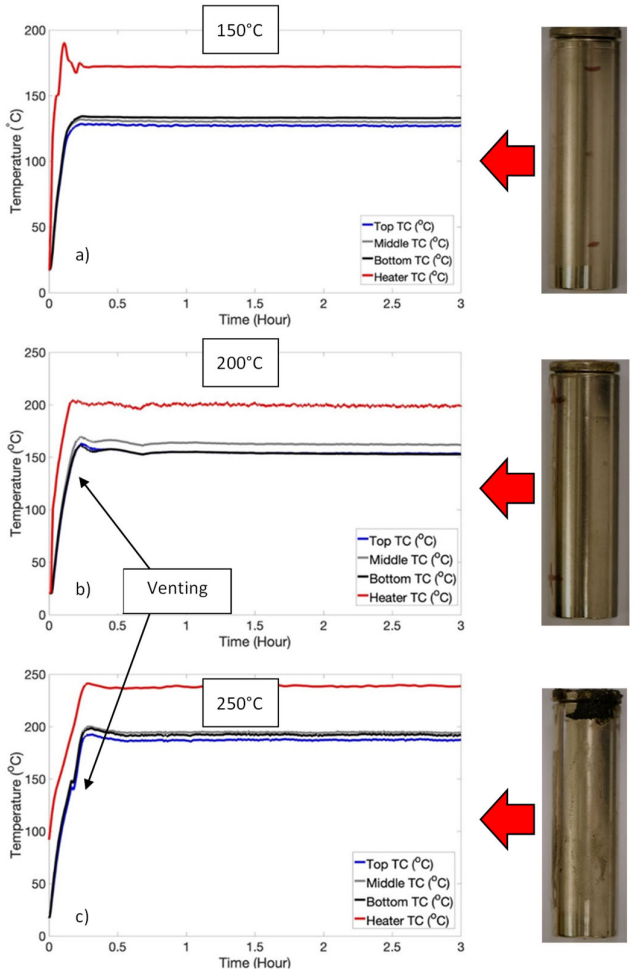

Figure 2. Temperature plots and images after testing for low SOC test. Typical plots and images are shown after the test for 150°C a), 200°C b), and 250°C c).

3.2. Triggering of Thermal Runaway: High SOC Regime

Thermal runaway has been commonly identified by an increase in temperature greater than 2°C min^{-1} by accelerated rate calorimetry testing [25]. Alternatively, thermal runaway can be identified by a cascade of exothermic reactions which lead to high temperatures and subsequent catastrophic cell failure [11]. This event involves a significant amount of damage to the cell.

Both venting and thermal runaway were observed in high SOC testing; with heater temperatures of 200°C and 250°C required for these thermal events (refer to Table 2). Typical temperatures measured during high SOC testing are shown by Figure 3. Temperatures applied uniformly to the cell (via safety testing) are significantly lower than those applied to induce venting and thermal runaway in this work. This is due to the localised nature of heating whereby heat dissipates from areas not in contact with the heater. The temperature of the cell will increase where the heat generation exceeds the rate of heat dissipation.

Thermal gradients were observed axially as well as longitudinally on the cell can via selectively placed TCs (refer to Figure 1). The heater TC had the highest temperature until thermal runaway, at which point the TC on the opposite side registered the highest temperature indicating TR had initiated inside the can. In the 200°C test, temperatures of up to 650°C were logged and in the 250°C test, up to 480°C was logged.

 doi:10.20944/preprints202402.0095.v1

Table 2. Summary of testing results.

Test	Temperature (°C)	Events
High SOC	100	Nil
	150	Nil
	200	Venting and TR
	250	Venting and TR

Other studies have shown thermal runaway temperatures on the cell surface of up to 650°C [28]. Given the violent nature of the reactions involved thermal runaway and the significant amount of damage observed in the 250°C cell due to testing, it is likely that the TCs detached from the cell surface causing lower than expected temperatures.

Studies have shown cell surface temperatures monitored where heating is applied rapidly to the cylindrical cell base using a heat gun [29]. With temperatures >250°C venting and thermal runaway was induced due to localised hotspots. These hotspots were deemed to be caused by severe short circuits whereby a short-lived release of energy causes thermal runaway. The event that caused this shorting was thought to be via dendrite growth, impurities in the cell or by internal structural collapse because of contact between highly conductive layers (the current collectors for example). At high SOC cells are more likely to undergo thermal runaway with an internal short circuit (ISC) [30].

Short circuits have been induced (by ISC devices) near to the sidewall and have led to sidewall bursting [31]. These devices provide an electronically conductive path between the negative carbon electrode and the positive aluminium current collector. However, they do not simulate the process of separator melting and shorting via the anode and cathode coming into contact. No sidewall bursts were observed in this study, though this is likely due to the thickness of the cell wall, as discussed below.

 doi:10.20944/preprints202402.0095.v1

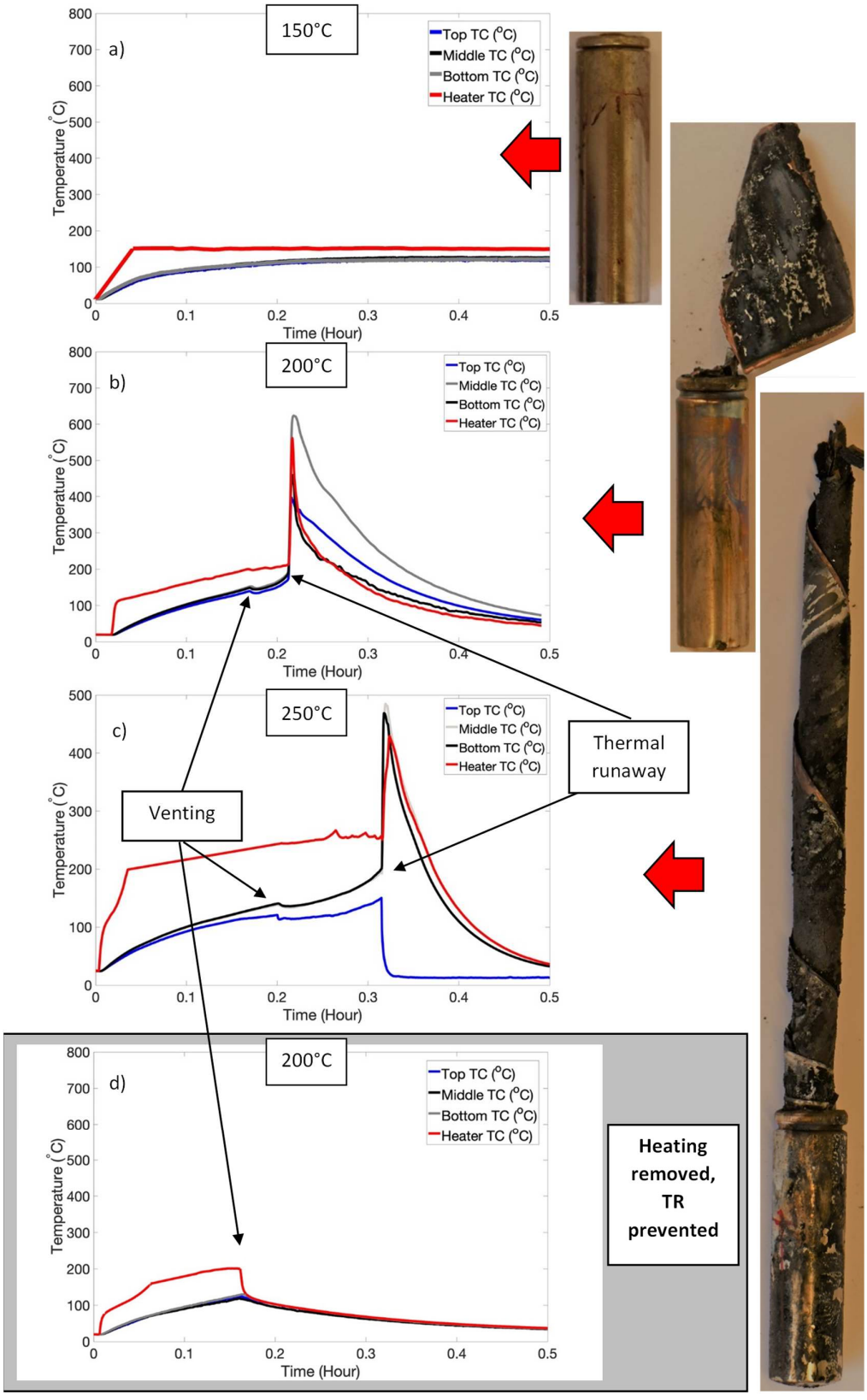

Figure 3. Temperature plots and images after testing for high SOC test, for a) 150°C, b), 200°C and c) 250°C. d) shows a typical plot at 200°C when heating was removed after venting preventing TR.

 doi:10.20944/preprints202402.0095.v1

A definitive time lag is observed between the venting event and thermal runaway events, suggesting that additional heat was required to induce TR. To explore the possibility that removing the heat source from the cell would eliminate resulting TR, the test was repeated at 200°C with heat removed from the cell once venting had occurred. This is shown by Figure 3d. This has important ramifications, in that by removing the heat source (or quenching) following venting, TR can be prevented, provided that self-heating hasn't started.

3.3. Implications of NMC Cathode Chemistry on TR

As previously mentioned, the thermal stability of NMC and the anode's SOC are instrumental to the severity of TR [14]. In this particular type of LG cylindrical cell the cathode is NMC532 ($Li(Ni_{0.5}Mn_{0.3}Co_{0.2})O_2$). When comparing cathode chemistries, the thermal stability order of different cathode structures has been reported to follow the trend (at full SOC): LFP > LMO > NMC > NCA > LCO, with the latter being the least stable [32].

Within the NMC family of materials, Ni is the most thermally reactive element in terms of redox dynamics, with Mn being the more redox-stable element. NMC 532 is considered to be a good compromise between thermal stability and capacity compared with the other members of the NMC series [33]. Charged NMC532 follows a specific path of phase transitions during thermal decomposition:

$$\text{(i) } LiTMO_2 \rightarrow LiTM_2O_4 \text{ (starting at ca. } 235^oC) \text{ [33]}$$

$$\text{(ii) } LiTM_2O_4 \rightarrow LiTMO$$

These transitions are temperature dependent and correlate with reduction of O:M stoichiometry due to oxygen loss. Compared with NMC333 and 433, NMC 532 has been reported to have better thermal stability, with x-ray diffraction (XRD) and mass spectroscopy (MS) studies demonstrating that thermal stability dramatically deteriorates when the Ni composition changes from NMC 532 to 622 [20,33]. However, such correlations have been questioned based on comparisons being performed after charging to an equal upper cut-off potential [34,35]. On the basis of analytical verification, the variations in specific capacity originate from different Li^+ extraction ratios, which can predominantly influence the structural stability of layered transition metal oxides [36]. For this reason, the term stability should take into account structural stability with respect to Li extraction, but also thermal stability, which is dependent on Ni content, electrolyte and SOC. Figure 4 depicts a series of stages known to occur during the initial stages of TR in NMC-graphite cells at high SOCs, and can be regarded as co-dependent degradation, linking the anode and cathode. The cascade of reactions begins with the thermal decomposition of the passivating SEI layer on the anode, which can begin at around 90°C [37]. This is the first stage of the cell's self-heating behaviour and will be followed by further reactions between the electrolyte and intercalated Li (when at a higher SOC), which is an exothermic process and can cause secondary SEI growth [38].

Preprints.org (www.preprints.org) | NOT PEER-REVIEWED | Posted: 2 February 2024 doi:10.20944/preprints202402.0095.v1

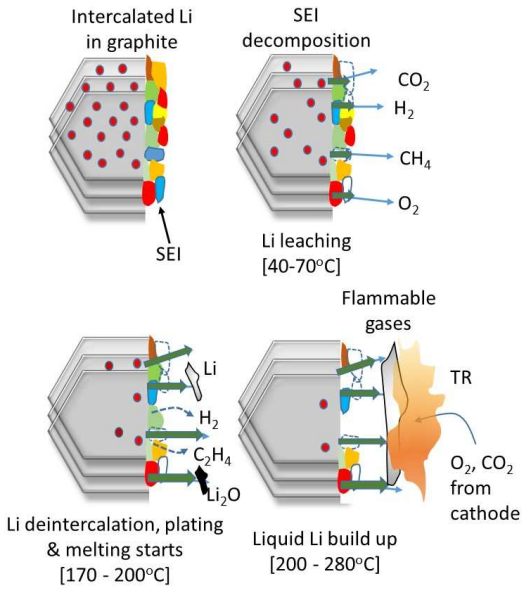

Figure 4. Implication of anode high SOC on the onset events leading to TR.

SEI reformation can lead to carbonate species disappearing and inorganic species increasing – such sequences have been referred to as a chain reaction of parasitic exothermic reactions [14]. This will continuously drive the elevation of the cell's temperature.

At this point the separator will already have started shrinking increasing the likelihood of a short-circuit (refer Figure 5a). When the temperature exceeds 200°C (as is induced in our study) the cathode starts to decompose, accelerating structural decomposition and oxygen release [39]. Localised heating triggers the loss of transition metal (TM) cations by breaking the TM-O bonds, leading to O-O bond formation between the under co-ordinated oxygen atoms - this results in parasitic oxygen release [40,41]. In layered oxide materials the activation energy of oxygen release has been found to be a function of the SOC and extent of delithiation, as previously mentioned [42]. As the released oxygen causes chemical oxidation of the electrolyte, the amounts of CO_2 and CO are generated simultaneously and will increase in volume with increasing temperature [43]. The adverse effects of CO_2 consumption was initially suggested to cause shuttle reactions between cathodes and anodes, whereby molecular CO_2 reacts with deintercalated Li^+ to form lithium oxalate ($Li_2C_2O_4$) [44]. When this species thermally decomposes the reaction is highly exothermic (<585°C)[45] and would certainly constitute a dominant self-heating source. However, Girgis [45] also claimed that significant formation of this species was unlikely to occur in commercial cells. In short, there are a variety of chemical cross-talk possibilities between the anode and cathode that culminate in TR, with cathode-released oxygen consumption by the charged anode being a significant stage [14]. Other studies have highlighted that hydrogen is implicated as being one of the critical flammable gas species involved in TR -with initial release triggered by SEI breakdown, then at higher temperatures about 170°C by the breakdown of polyvinylidene fluoride (PVdF) [46]. The mechanistic elucidation and quantification of species formed during TR onset is incredibly complex, and still far from being fully resolved and will be considered in separate studies the scope of this investigation. A question that remains is at what point do the heat generating reactions within the cell make TR inevitable? Previous temperature vs time plots show a definite time lag between the venting event and the thermal runaway event. This suggests additional (applied) heat was required to induce these internal exothermic reactions after venting so as to induce TR. Figure 5 shows the TR cascade of reactions (a) and the temperature plots of TR and venting.

 doi:10.20944/preprints202402.0095.v1

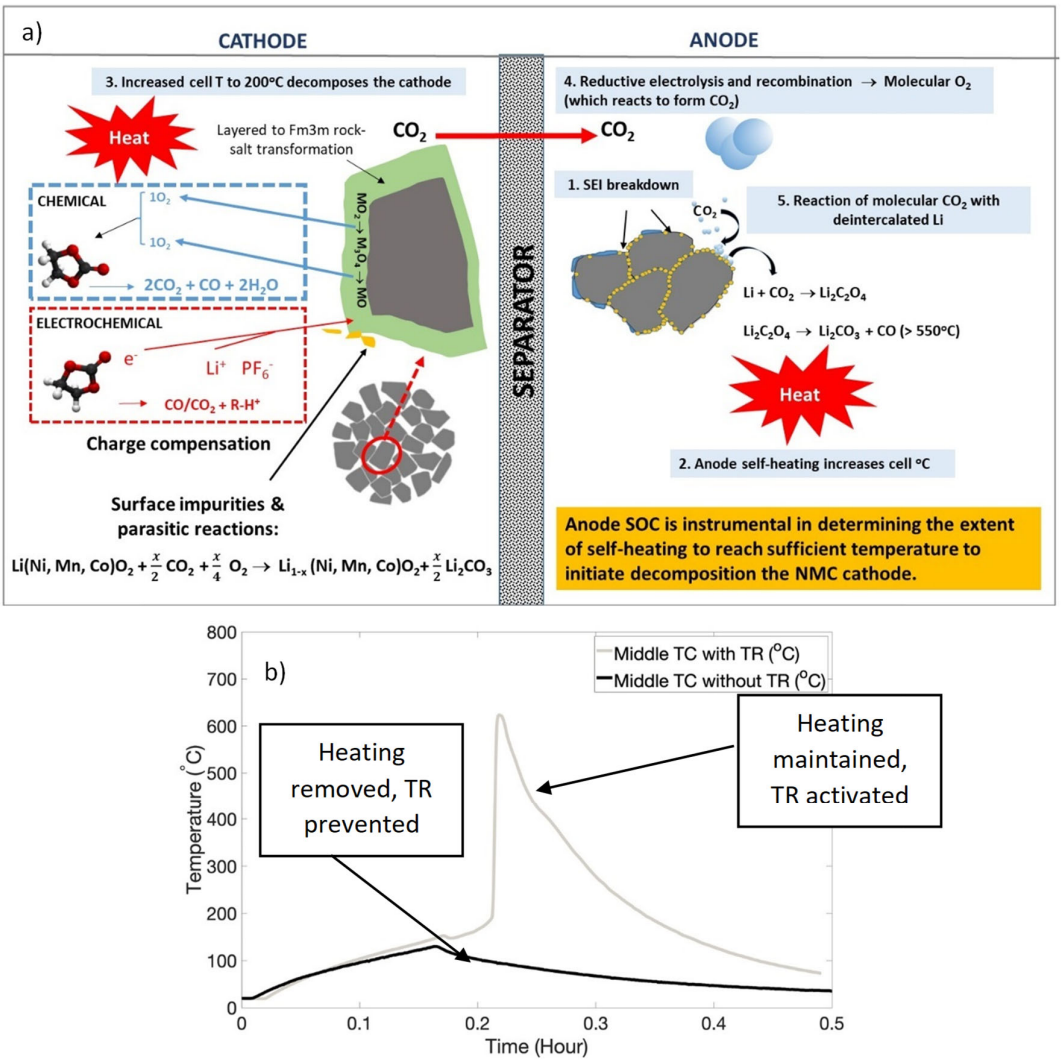

Figure 5. a) Decomposition cascade highlighting co-dependent behaviours of anodes and cathodes during cell heating; b) temperature plots for cells with high SOC and 200°C with and without TR activation.

As shown by Figure 5b, by removing the heater we were able to prevent TR, such that the internal heat generating reactions (such as the cathode decomposition) were not activated. Other cooling mechanisms (such as water quenching) could also be applied at this time to further retard TR. The catastrophic nature of TR would be prevented by these actions, thus ensuring safety.

3.4. Examination of Cells Following Thermal Runaway

Cells that underwent venting and TR in the high SOC test exhibited significant charring and oxidation; indicators that the cell had ignited and combusted. The combustion process for localised heating to the side of a cylindrical cell has been described previously [26] as continuous heating and self-heating, rupture and ignition, violent ejection or explosion, relatively less violent combustion and flame weakening and extinguishing.

Cells are termed as "burst" when ejection of components is uncontrolled of both the header components and the jelly roll from within the cell [47]. Controlled ejection (venting) involves retaining the header components intact, whilst allowing fluids to escape. Cells that had undergone TR experienced the jelly roll componentry exiting through the cell top (refer Figure 3). In the 250°C

 doi:10.20944/preprints202402.0095.v1

test the jelly roll extended to four times the length of the cell, which was twice the length of ejection in the 200°C cell. This implies that higher applied temperatures caused higher pressures within the cell since the jelly roll exited the cell to a greater length.

X-ray tomography has been used extensively to identify damage induced within cells [48,49]. Extensive damage to the jelly roll is shown in the samples that underwent TR (refer Figure 6). The gases generated induced a significant amount of stress to the jelly roll layers, causing them to plastically deform and become wave-like. There is a significant amount of void space in the cells, particularly in the 250°C cell due to the ejection of the jelly roll through the top of the cell. Bulging was noticed at the cell base in both the 200°C and 250°C cells. The aforementioned pressures were high enough to cause plastic deformation (i.e. bulging) of the cell can at this location, though not high enough to rupture the cell wall. More detail on how the pressures cause material stresses within the cell is described below.

The application of heat to one side of the cell did not appear to lead to any anisotropic damage features. The localised heating induced thermal runaway, pressure increase within the cell until the cell cap was detached and the jelly roll spiralled out of the cell. In a similar study, cells were shown to undergo venting from an application of 100°C temperature [29]. This caused the formation of gas pockets within the jelly roll. Shortly after venting, the jelly roll became severely deformed and collapsed into the void space at the centre of the cell. This collapse led to many 'kinks' within the jelly roll which would likely cause short circuiting due to damage to the separator.

This collapse of the electrode assembly into the vacant core of the cell has been observed in high current aging studies [50,51], likely to be due to thermal stresses between a (hot) inside and a (cold) outside of the cell resulting in plastic deformation of the jelly roll layers into the vacant core. The presence of a centre mandrel has shown to inhibit these jelly roll deformations. It is also believed that having a central mandrel aides the release of pressure within the cell as well as making a clear path for fluidised material in venting and thermal runaway [48]. This collapse of the jelly roll into the void space at the centre of the cell is assumed to have occurred here, since there was no centre mandrel. It is thought that collapse creates a more tortuous path for gas evolution within the cell, increasing the risk of cell bursting due to clogging the gas flow to the top of the cell. No sidewall failures occurred in this study, which would likely be one of the effects of this event.

The cell contained both a positive temperature coefficient (PTC) switch and a current interrupt device (CID) at the top (positive) end of the cell. The PTC switch is primarily designed to prevent external short circuits as well as to protect against electrical abuse [52]. This is accomplished by an increase in electrical resistance at elevated temperatures; whereby current flow to the cell is limited [3]. The CID device is a concave domed disc. In response to pressure build-up within the cell, this disk firstly becomes convex and then secondly ruptures at a certain pressure initiating the venting process.

TR also stretched the spin groove of the crimp seal such that the crimp angle at the top of the cell was increased. The can at this location was plastically deformed (with the tensile strength of the can exceeded at this location) due to the pressure developed within the cell. The spin groove has been thought to determine the volume of gases that can accumulate in the cell before bursting [48].

As mentioned previously, temperatures experienced within the cell are believed to be significantly higher than those applied on the outside of the cell. The tomograms show dense materials which are indicated by bright regions; such as the copper current collector. With high applied temperatures the copper has melted and re-solidified into smaller spheres, which are the highly attenuating globules indicated by green arrows in Figure 6. Internal temperatures must have reached at least 1085°C; the melting point of copper. This supports other claims of internal temperature > 1000°C during thermal runaway [53].

 doi:10.20944/preprints202402.0095.v1

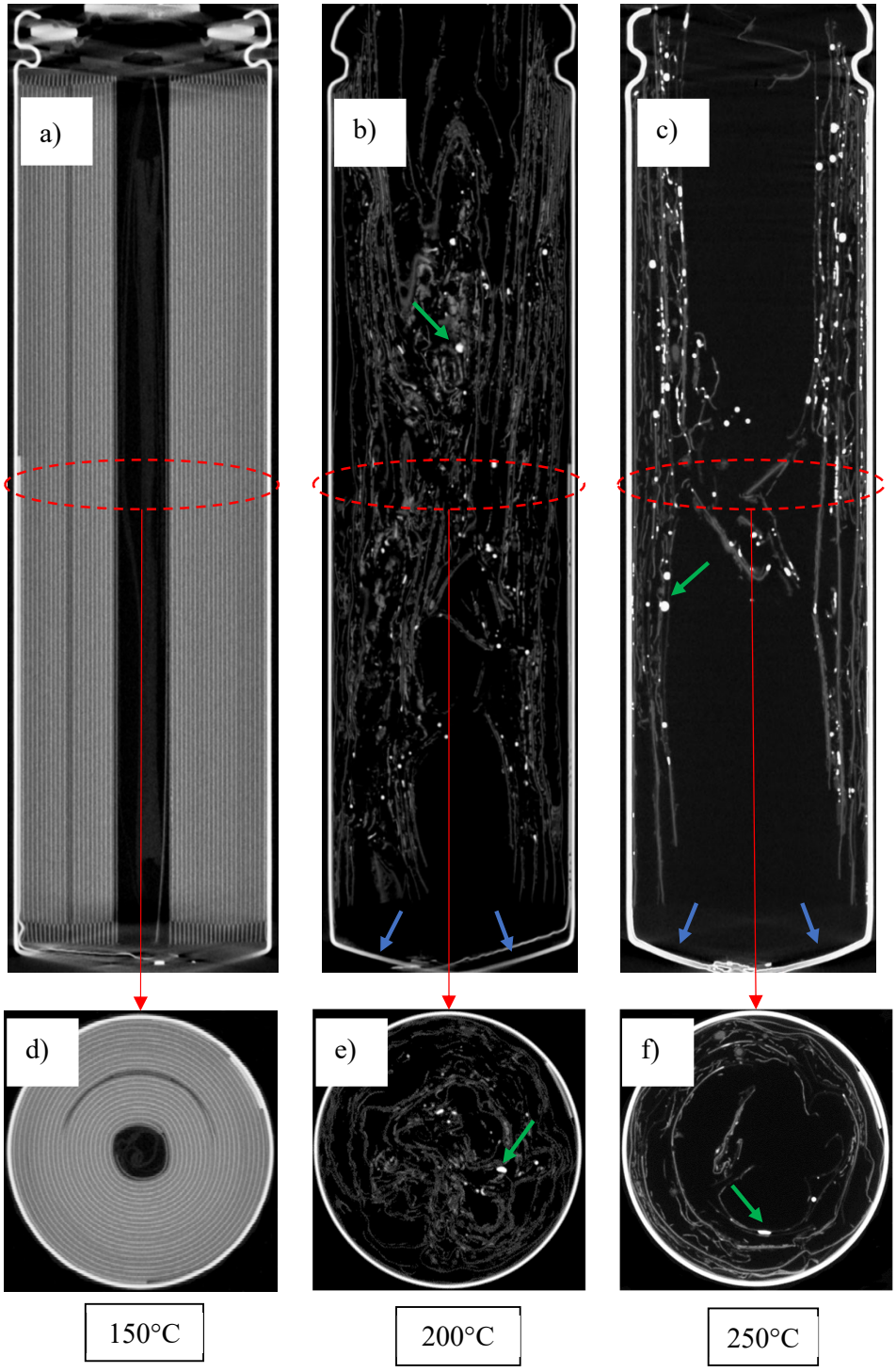

Figure 6. Tomograms of cells after testing. Longitudinal scans shown by a), b) and c). Axial scans shown by d), e), and f). Blue arrows show bulging and green arrows show examples of melted copper.

The mechanical degradation of the cell can after the high SOC test was evaluated by hardness testing. Testing was carried out on the can at the middle of the heater; with five indents taken at the front and the back of the cell. Hardness values were averaged at these locations and compared for the various temperatures applied in the cell heating test. Figure 5 shows the results for these tests. The thermal profiles solely applied by the heater did not change the mechanical properties of the can.

 doi:10.20944/preprints202402.0095.v1

Rather, it was the thermal runaway event that changed the hardness; the can became softer. Hardness testing is directly proportional to the yield strength of a material [54].

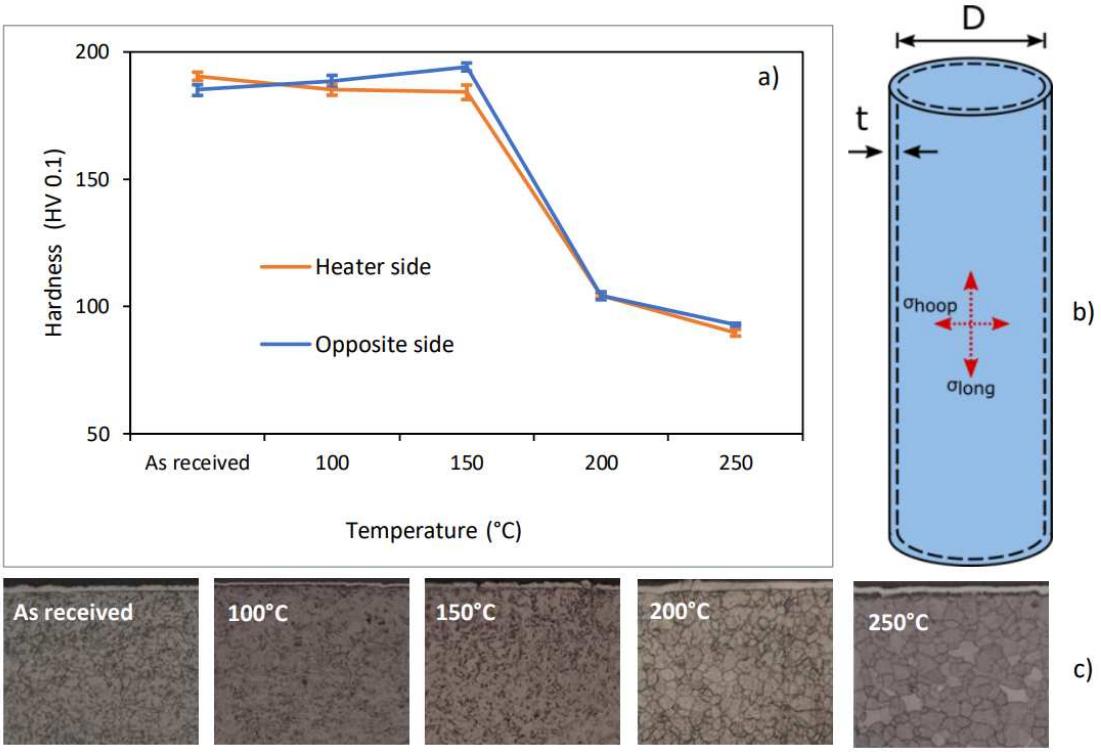

Figure 7. Mechanical degradation and design of cylindrical cell. a) shows average mechanical properties of the cell can, b) shows mechanical design and associated stresses, and c) shows typical microstructure.

The tensile strength of steel has been shown to decrease rapidly at temperatures > 100°C [47], which would increase the likelihood of the can rupturing. This was not observed here, the tensile strength of the can was maintained in cells that were exposed to the heating temperatures until the TR event occurred. This softening of the can material was due to exposure to temperatures up to 700°C. Furthermore, weakening of the casing has been discussed and associated with sidewall rupture [31]. In this study, no sidewall ruptures were observed.

The cell can microstructure changed noticeably as a result of TR. Samples of as-received cell cans are fabricated from Ni-plated steels with microstructure comprising of cold-worked ferrite grains. These ferrite grains recrystallised and became equiaxed with thermal runaway. In carbon steel, recrystallisation occurs at 721°C [55]; higher temperatures than what was measured by TCs on the outside of the cell.

The design of the cylindrical cell is analogous to a thin-walled pressure vessel [56]. With some applied internal pressure, the stresses can be resolved into a longitudinal stress (σ_{long}) and a hoop stress (σ_{hoop}) acting on the cell ends and radially respectively (refer Figure 5b).

This longitudinal stress and hoop stress within the cell described by Equation 1 and 2 respectively.

$$\sigma_{long} = \frac{pD}{4t} \quad (1)$$

$$\sigma_{hoop} = \frac{pD}{2t} \quad (2)$$

 doi:10.20944/preprints202402.0095.v1

where σ_{long} = longitudinal stress (MPa), p = internal pressure (MPa), D = internal diameter (mm), t = wall thickness (mm) and σ_{hoop} = hoop stress (MPa). As can be seen by the equations, the hoop stress is twice the longitudinal stress. Furthermore, where the cylinder is sufficiently long the hoop stress is known to be the predominant stress acting upon the cylinder.

The CID device is designed to break in the event of pressure increase within the cell at some (longitudinal) stress, releasing gas into the surroundings. In this way pressures (and high stresses) that lead to an explosion (and catastrophic failure) can be avoided. Similar engineering controls are adopted in the power industry [57]. Pressure piping is designed to 'leak before burst' which allows time for the detection of leaks from a pipe before it bursts such that the piping can be switched off. Similarly, catastrophic failure is avoided.

Sidewall breaches are known to be one of the worst failure scenarios [31,47], and will occur where the hoop strength of the can has been exceeded by internal pressure. This scenario was not observed in the testing carried out. This indicates the wall thickness of the can was sufficient to withstand the hoop stresses. Furthermore, with the venting mechanism being designed to be the limiting factor in the event of pressure build-up; it indicates the cell was designed to withstand the correct ratio of longitudinal stress to hoop stress.

3.5. Released Gas Analysis

Gases were formed by various decomposition reactions inside the cell and released in venting and TR events. These gases were initially formed by reactions inside the cell as already mentioned and include the decomposition of several components: SEI, electrolyte, cathode material, binder and also solvents. Figure 8 shows the typical spectra for the gases observed in high SOC test with an applied 200°C. The gases detected include CH_4, C_2H_4, C_2H_6, C_3H_8, H_2, H_2O, CO, O_2, and CO_2. Additionally, as the experiment was carried out in open atmosphere, atmospheric gases (N_2, O_2, CO_2, and Ar) were also detected. Other studies [58] have found many gas species (>100) during thermal runaway due to many reactions occurring at high temperatures. However, this experiment was undertaken in a closed vessel. Since our experiment was carried out in open atmosphere, with the gas analyser at a distance from the cell top, only qualitative analysis was possible. It is likely that in this situation only the gases in high concentrations were detected (including O_2 and N_2). Commercial NMC cells were investigated versus other chemistries (LFP, LTO) in a separate study [59] and the NMC cell produced the largest pressure during TR. The major gases analysed here align with the findings in Figure 8a, showing significant peaks of gas species attributable to CO and C_2H_4.

 doi:10.20944/preprints202402.0095.v1

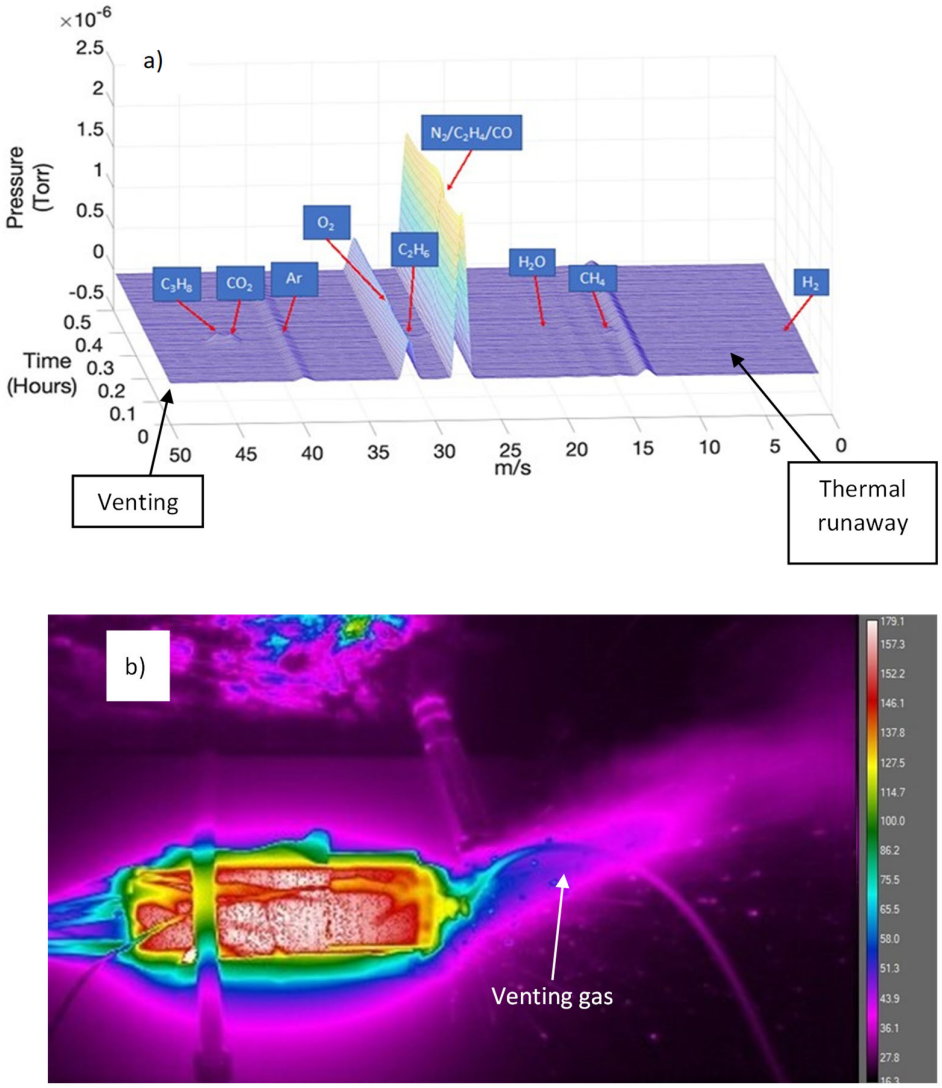

Figure 8. Results from gas analysis. a) shows GC-MS spectra for high SOC test at 200 °C and b) shows thermographic image taken during venting.

The gases detected (CO and C_2H_4) during the venting and TR events were likely to be related to the breakdown of the SEI within the cell and related cathode shuttle mechanisms as outlined in Figure 5.

4. Conclusions

In this study we have focused on the significant interplay between cell SOC and temperature towards the nature of thermal failure in lithium-ion cells. By simulating a realistic thermal scenario, by applying an external temperature to the outside of the cell, we monitored the cell until it reached eventual TR. It is already known from other studies that the decomposition of the anode is the critical driver for TR onset via a self-heating mode, which drives the decomposition of the cathode via a series of 'shuttle' stages. At high SOC whereby the graphite is lithiated, this will increase the rate of self-heating. By allowing continued exothermic anode decomposition, catastrophic failure will result. We demonstrate that by implementing a simple convection cooling mechanism - removing the heat source - we could suppress TR.

This practical solution warrants the investigation of other quenching methods that can be activated when the temperature exceeds a critical threshold. Such studies serve to better inform

improving development in thermal management systems for example better distribution of effective refrigerants or use of improved heat-dissipating materials. Vital to activating such mechanisms will be continued advancing of temperature sensing capable of fast detection and precise measurement. Underpinning such technology developments with forensic simulations is an effective approach for resolving when and how to implement better safety controls. This will ultimately serve to mitigate catastrophic failure in cells and modules and will become more critical as we continue to increase cell format sizes and higher energy density electrodes.

Author Contribution: Justin Holloway: Conceptualization, Methodology, Validation, Investigation, Resources, Writing - Original Draft, Supervision, Project administration, Funding acquisition. **Muinuddin Maharun:** Software, Formal analysis, Investigation, Writing - Original Draft, Writing - Review & Editing. **Irma Houmadi:** Investigation. **Guillaume Remy:** Investigation. **Louis Piper**: Writing - Review & Editing, Visualization. **Mark Williams:** Writing- Reviewing and Editing, **Melanie Loveridge:** Writing - Review & Editing, Visualization.

Acknowledgments: The research was undertaken in collaboration with the WMG Centre High Value Manufacturing Catapult (funded by Innovate UK). We acknowledge the Faraday Institution's Degradation and SafeBatt projects, grant references RG94392 FRIG024 and FIRG061. The authors would also like to acknowledge the National Research Facility in x-ray Computed Tomography (NXCT) grant reference EP/T02593X/1.

Declaration of Competing Interest: There is no conflict of interest in this manuscript.

Glossary

CC = constant current
CV = constant voltage
C = coulomb
NMC = lithium nickel cobalt manganese oxide
SEI = solid electrolyte interphase
SOC = state of charge
TR = thermal runaway
LIB = lithium ion battery
BMS = battery management system
TC = thermocouple
PID = proportional integral derivative controller
CID = current interrupt device
PTC = positive temperature coefficient device
QMS = quadrupole mass spectrometer
PCB = printed circuit board
ISC = internal short circuit
XRD = x-ray diffraction
MS = mass spectroscopy
TM = transition metal
PVdF = polyvinylidene fluoride
NDT = non-destructive testing

References

1. Koch, S., Fill, A. & Birke, K. P. Comprehensive gas analysis on large scale automotive lithium-ion cells in thermal runaway. *J. Power Sources* **398**, 106–112 (2018).
2. Xu, K. Nonaqueous liquid electrolytes for lithium-based rechargeable batteries. *Chem. Rev.* **104**, 4303–4417 (2004).
3. Lisbona, D. & Snee, T. A review of hazards associated with primary lithium and lithium-ion batteries. *Process Saf. Environ. Prot.* **89**, 434–442 (2011).
4. Advanced Science - 2017 - Finegan - Identifying the Cause of Rupture of Li-Ion Batteries during Thermal Runaway.pdf.
5. Hou, J. *et al.* Thermal runaway of Lithium-ion batteries employing LiN(SO2F)2-based concentrated electrolytes. *Nat. Commun.* **11**, 1–11 (2020).

6. Cai, T. *et al.* Detection of Li-ion battery failure and venting with Carbon Dioxide sensors. *eTransportation* **7**, 100100 (2021).
7. Gao, A., Xu, F. & Dong, W. The Concept of early monitoring and warning of thermal runaway of lithium-ion power battery using parameter analysis. *J. Phys. Conf. Ser.* **2181**, (2022).
8. Adv Energy and Sustain Res - 2021 - McKerracher - Advances in Prevention of Thermal Runaway in Lithium-Ion Batteries.pdf.
9. Srinivasan, R. *et al.* Review—Thermal Safety Management in Li-Ion Batteries: Current Issues and Perspectives. *J. Electrochem. Soc.* **167**, 140516 (2020).
10. Golubkov, A. W. *et al.* Thermal-runaway experiments on consumer Li-ion batteries with metal-oxide and olivin-type cathodes. *RSC Adv.* **4**, 3633–3642 (2014).
11. Spotnitz, R. & Franklin, J. Abuse behavior of high-power, lithium-ion cells. *J. Power Sources* **113**, 81–100 (2003).
12. Authorized, N. O. T., Further, F. O. R., Or, R., Without, D. & From, P. *Household and Commercial Batteries*.
13. Bareño, J. *et al.* Effect of overcharge on Li(Ni0.5Mn0.3Co0.2)O2/graphite lithium ion cells with poly(vinylidene fluoride) binder. III — Chemical changes in the cathode. *J. Power Sources* **385**, 165–171 (2018).
14. Liu, X. *et al.* Thermal Runaway of Lithium-Ion Batteries without Internal Short Circuit. *Joule* **2**, 2047–2064 (2018).
15. Mendoza-Hernandez, O. S., Ishikawa, H., Nishikawa, Y., Maruyama, Y. & Umeda, M. Cathode material comparison of thermal runaway behavior of Li-ion cells at different state of charges including over charge. *J. Power Sources* **280**, 499–504 (2015).
16. Gilbert, J. A. *et al.* Cycling Behavior of NCM523/Graphite Lithium-Ion Cells in the 3–4.4 V Range: Diagnostic Studies of Full Cells and Harvested Electrodes. *J. Electrochem. Soc.* **164**, A6054–A6065 (2017).
17. Wu, L. *et al.* Structural origin of overcharge-induced thermal instability of Ni-containing layered-cathodes for high-energy-density lithium batteries. *Chem. Mater.* **23**, 3953–3960 (2011).
18. Shu, J. *et al.* In-situ X-ray diffraction study on the structural evolutions of LiNi 0.5Co0.3Mn0.2O2 in different working potential windows. *J. Power Sources* **245**, 7–18 (2014).
19. Zheng, Y. *et al.* Influence of over-discharge on the lifetime and performance of LiFePO4/graphite batteries. *RSC Adv.* **6**, 30474–30483 (2016).
20. Li, T. *et al. Degradation Mechanisms and Mitigation Strategies of Nickel-Rich NMC-Based Lithium-Ion Batteries*. *Electrochemical Energy Reviews* vol. 3 (Springer Singapore, 2020).
21. Zeng, X., Zhan, C., Lu, J. & Amine, K. Stabilization of a High-Capacity and High-Power Nickel-Based Cathode for Li-Ion Batteries. *Chem* **4**, 690–704 (2018).
22. Shizuka, K., Kiyohara, C., Shima, K. & Takeda, Y. Effect of CO2 on layered Li1+zNi1-x-yCoxMyO2 (M = Al, Mn) cathode materials for lithium ion batteries. *J. Power Sources* **166**, 233–238 (2007).
23. Wang, D. *et al.* Effect of high Ni on battery thermal safety. *Int. J. Energy Res.* **44**, 12158–12168 (2020).
24. Tan, C. C. *et al.* Ageing analysis and asymmetric stress considerations for small format cylindrical cells for wearable electronic devices. *J. Power Sources* **472**, 228626 (2020).
25. Lammer, M., Königseder, A. & Hacker, V. Holistic methodology for characterisation of the thermally induced failure of commercially available 18650 lithium ion cells. *RSC Adv.* **7**, 24425–24429 (2017).
26. Chen, M., Liu, J., He, Y., Yuen, R. & Wang, J. Study of the fire hazards of lithium-ion batteries at different pressures. *Appl. Therm. Eng.* **125**, 1061–1074 (2017).
27. Somandepalli, V., Marr, K. & Horn, Q. Quantification of combustion hazards of thermal runaway failures in lithium-ion batteries. *SAE Int. J. Altern. Powertrains* **3**, 98–104 (2014).
28. Finegan, D. P. *et al.* Modelling and experiments to identify high-risk failure scenarios for testing the safety of lithium-ion cells. *J. Power Sources* **417**, 29–41 (2019).
29. Finegan, D. P. *et al.* In-operando high-speed tomography of lithium-ion batteries during thermal runaway. *Nat. Commun.* **6**, 1–10 (2015).
30. Doughty, D. & Roth, E. P. A general discussion of Li Ion battery safety. *Electrochem. Soc. Interface* **21**, 37–44 (2012).
31. Finegan, D. P. *et al.* Characterising thermal runaway within lithium-ion cells by inducing and monitoring internal short circuits. *Energy Environ. Sci.* **10**, 1377–1388 (2017).
32. Furushima, Y., Yanagisawa, C., Nakagawa, T., Aoki, Y. & Muraki, N. Thermal stability and kinetics of delithiated LiCoO2. *J. Power Sources* **196**, 2260–2263 (2011).
33. Bak, S. *et al.* Structural Changes and Thermal Stability of Charged LiNi. *Appl. Mater. Interfaces* **6**, 22594–22601 (2014).
34. Kasnatscheew, J. *et al.* The truth about the 1st cycle Coulombic efficiency of LiNi1/3Co1/3Mn1/3O2 (NCM) cathodes. *Phys. Chem. Chem. Phys.* **18**, 3956–3965 (2016).
35. Shi, Y., Chen, G., Liu, F., Yue, X. & Chen, Z. Resolving the Compositional and Structural Defects of Degraded LiNixCoyMnzO2 Particles to Directly Regenerate High-Performance Lithium-Ion Battery Cathodes. *ACS Energy Lett.* **3**, 1683–1692 (2018).

36. Kasnatscheew, J., Röser, S., Börner, M. & Winter, M. Do Increased Ni Contents in LiNi xMn yCo zO2 (NMC) Electrodes Decrease Structural and Thermal Stability of Li Ion Batteries? A Thorough Look by Consideration of the Li+ Extraction Ratio. *ACS Appl. Energy Mater.* **2**, 7733–7737 (2019).
37. Adams, R. A., Varma, A. & Pol, V. G. Mechanistic elucidation of thermal runaway in potassium-ion batteries. *J. Power Sources* **375**, 131–137 (2018).
38. Mao, B., Huang, P., Chen, H., Wang, Q. & Sun, J. Self-heating reaction and thermal runaway criticality of the lithium ion battery. *Int. J. Heat Mass Transf.* **149**, 119178 (2020).
39. Advanced Energy Materials - 2019 - Sharifi-Asl - Oxygen Release Degradation in Li-Ion Battery Cathode Materials Mechanisms.pdf. *Adv. Energy Mater.* **9**, 1900551 (2019).
40. Yano, A., Shikano, M., Ueda, A., Sakaebe, H. & Ogumi, Z. LiCoO 2 Degradation Behavior in the High-Voltage Phase Transition Region and Improved Reversibility with Surface Coating . *J. Electrochem. Soc.* **164**, A6116–A6122 (2017).
41. Al, K.-W. N. Adv Func Combining In Situ Synchrotron X-Ray Diffraction and Absorption Techniques with.pdf. **23**, 1047–1063 (2013).
42. Sharifi-Asl, S., Lu, J., Amine, K. & Shahbazian-Yassar, R. Oxygen Release Degradation in Li-Ion Battery Cathode Materials: Mechanisms and Mitigating Approaches. *Advanced Energy Materials* vol. 9 (2019).
43. Jung, R., Strobl, P., Maglia, F., Stinner, C. & Gasteiger, H. A. Temperature Dependence of Oxygen Release from LiNi 0.6 Mn 0.2 Co 0.2 O 2 (NMC622) Cathode Materials for Li-Ion Batteries . *J. Electrochem. Soc.* **165**, A2869–A2879 (2018).
44. Ellis, L. D. *et al.* Quantifying, Understanding and Evaluating the Effects of Gas Consumption in Lithium-Ion Cells. *J. Electrochem. Soc.* **164**, A3518–A3528 (2017).
45. Girgis, M. M. & El-Awad, A. M. Kinetics and mechanism of thermal decomposition of lithium oxalate catalysed by Cd1-xCoxFe2O4(x =0.0, 0.5 and 1.0) ferrospinel additives. *Thermochim. Acta* **214**, 291–303 (1993).
46. Liu, X. *et al.* In situ observation of thermal-driven degradation and safety concerns of lithiated graphite anode. *Nat. Commun.* **12**, (2021).
47. Finegan, D. P. *et al.* Modelling and experiments to identify high-risk failure scenarios for testing the safety of lithium-ion cells. *J. Power Sources* **417**, 29–41 (2019).
48. Finegan, D. P. *et al.* Identifying the Cause of Rupture of Li-Ion Batteries during Thermal Runaway. *Adv. Sci.* **5**, (2018).
49. Yufit, V. *et al.* Investigation of lithium-ion polymer battery cell failure using X-ray computed tomography. *Electrochem. commun.* **13**, 608–610 (2011).
50. Holloway, J. *et al.* Determining the limits and effects of high-rate cycling on lithium iron phosphate cylindrical cells. *Batteries* **6**, 1–18 (2020).
51. Fleischhammer, M., Waldmann, T., Bisle, G., Hogg, B. I. & Wohlfahrt-Mehrens, M. Interaction of cyclic ageing at high-rate and low temperatures and safety in lithium-ion batteries. *J. Power Sources* **274**, 432–439 (2015).
52. Balakrishnan, P. G., Ramesh, R. & Prem Kumar, T. Safety mechanisms in lithium-ion batteries. *J. Power Sources* **155**, 401–414 (2006).
53. Golubkov, A. W. *et al.* Thermal runaway of commercial 18650 Li-ion batteries with LFP and NCA cathodes - Impact of state of charge and overcharge. *RSC Adv.* **5**, 57171–57186 (2015).
54. Jun, S. C. *Mechanical Testing and Evaluation*. *Graphene-based Energy Devices* (Wiley-VCH verlag GmbH & Co. KgaA, 2015).
55. Baker, H. *ASM Handbook, Volume 3: Alloy Phase Diagrams*. (ASM International, 1992).
56. Becker, W. et al. *ASM Handbook, Volume 11: Failure Analysis and Prevention*. (2002).
57. Cartwright, R. Book Reviews: Book Reviews. *Perspect. Public Health* **130**, 239–239 (2010).
58. Sun, J. *et al.* Toxicity, a serious concern of thermal runaway from commercial Li-ion battery. *Nano Energy* **27**, 313–319 (2016).
59. Yuan, L., Dubaniewicz, T., Zlochower, I., Thomas, R. & Rayyan, N. Experimental study on thermal runaway and vented gases of lithium-ion cells. *Process Saf. Environ. Prot.* **144**, 186–192 (2020).